MODIFICATION OF ICA FOR EXTRACTING BLOOD VESSEL-RELATED COMPONENT IN NUCLEAR MEDICINE: CONTRAST FUNCTION AND NONNEGATIVE CONSTRAINTS

Mika Naganawa[1], *Yuichi Kimura*[2], *and Ayumu Matani*[1]

[1]Dept. of Complexity Science and Engineering,
Graduate School of Frontier Sciences, University of Tokyo
7-3-1, Hongo, Bunkyo, Tokyo, 113-0033, Japan
[2]Positron Medical Center, Tokyo Metropolitan Institute of Gerontology
1-1, Naka, Itabashi, Tokyo, 173-0022, Japan
E-mail: mika@isp.ac

ABSTRACT

The problem of extracting a blood vessel-related component from dynamic brain PET images is similar to the ICA analysis of fMRI data. Unique characteristics of this problem are: (1) the spatial distribution of vessels can be acquired by PET, and therefore the property of the probability distribution of the vessel component is known; and (2) independent maps and the mixing matrix are all nonnegative. We have proposed a method for extracting the pTAC based on ICA (EPICA). EPICA is a method designed for extracting the vessel component. We investigate (A) the variation of the estimated pTAC with changing parameters of a contrast function of EPICA, and (B) the effect of the nonnegative constraints in ICA using the ensemble learning algorithm. Our results show that (A) a penalty term influences the tail of the estimated pTAC, and (B) a nonnegative assumption in ICA is feasible for extracting a vessel component.

1. INTRODUCTION

An aim of this study is to propose a practical modification of independent component analysis (ICA) in nuclear medicine. In positron emission tomography (PET), radioisotpe labeled pharmaceutical is administrated to a patient, and its kinetic in a tissue can be measured as a spatial distribution of radioactivity. For fully quantitative measurement, a relationship in concentration history of radioactivity between in an arterial blood and in target organs should be investigated using a compartment model [1]. This data analysis is known as a kinetic analysis and it enables the various functionalities in living tissue to be visualized. For example, 2-deoxy-2-^{18}F-fluoro-D-glucose (FDG) is used for the measurement of the regional cerebral metabolism of glucose. In the compartment model, the input and output functions are time courses in plasma of arterial blood (plasma time–activity curve; pTAC) and in a target tissue (tissue time–activity curve; tTAC), respectively. In an actual PET measurement, serial arterial blood sampling by a catheter inserted in a radial artery is required to measure pTAC. However, this is often a cumbersome operation and may result in infection, bleeding, and thrombosis [2][3]. Therefore, it is a serious problem to obtain pTAC without serial arterial blood sampling.

The previously reported algorithm to estimate pTAC from dynamic cardiac PET images is factor analysis of dynamic structures (FADS) [4][5][6]. FADS performs principal component analysis (PCA) and oblique rotations. The volume ratio of blood vessels to whole brain is approximately three percent in human FDG-PET images [7] and there are no voxels filled only with blood; therefore variance of the pTAC map is so small that FADS cannot estimate pTAC properly. In this paper, dynamic PET images are assumed to be decomposed into independent source maps (pTAC map and tTAC map), and pTAC is extracted as a column of the estimated mixing matrix using a spatial ICA.

Spatial ICA has been proposed for the extraction of the artifacts, or task-related activations from dynamic functional magnetic resonance imaging (fMRI) data [8]. The pTAC extraction algorithm is conceptually similar to the ICA analysis of fMRI. The differences between the two problems are:

(1) The statistical properties of pTAC and tTAC maps

This work is supported in part by the Grant-in-Aid for Scientific Research by Japan Society for the Promotion of Science, No. 13670977 in 2001 and 2002.

are available, which can be measured using ^{15}O-CO inhalation by PET [7]. Therefore, the statistical properties of the pTAC component can be assumed based on the measured data. In fMRI, artifacts or task-related activations are unknown.

(2) The signs of fMRI data can be both positive and negative, while the elements of the mixing matrix (pTAC and tTAC) and source matrix (pTAC and tTAC maps) should be all nonnegative.

As pTAC cannot be estimated successfully using conventional ICA [9], an appropriate transformation of brain PET images to satisfy the assumptions of ICA and design of a contrast function for extracting pTAC are required. We have proposed a novel method for extracting the pTAC-related component based on FastICA [10]: extraction of the pTAC using ICA (EPICA) [9][11]. EPICA performs the appropriate preprocessing (negative images and difference enhanced images) and spatial ICA using a contrast function designed for extracting the pTAC. The cost function of EPICA has two parameters, and we investigate the relation between the estimated pTAC and the shape of the cost function defined by the two parameters. The EPICA-estimated pTAC coincides closely to the measured pTAC; however, EPICA has an inherent problem in that ICA allows both signs in the estimated maps, although these should be nonnegative. Therefore, a nonnegative constraint should be incorporated into the estimation scheme for dynamic PET images. A recently developed ensemble learning (EL) algorithm for ICA assumes independent and nonnegative priors [12], which is therefore expected to overcome the problem of the sign of the maps. In this study, EPICA and EL for ICA are applied to FDG-PET images, and we will discuss the possibility that the nonnegative constraints extract more precise pTAC-related information.

2. MODEL

In a kinetic analysis in PET, a sequence of PET measurement is performed after administration of radiopharmaceutical. A voxel value at position q and frame f, $x(q,f)$, $(q = 1,\ldots,Q,\ f = 1,\ldots,F)$, is assumed to be a linear combination of pTAC, $c_{\rm p}(f)$, and tTAC, $c_{\rm t}(f)$, because a voxel covers both tissue and vessel. Figure 1 illustrates human brain FDG-PET images. Based on the compartment model [1], it is known that the relationship between pTAC, $c_{\rm p}(f)$, and tTAC, $c_{\rm t}(f)$, is:

$$c_{\rm t}(f) = \frac{K_1}{k_2+k_3}\left[k_3 + k_2\exp\left\{-(k_2+k_3)f\right\}\right] \otimes c_{\rm p}(f), \tag{1}$$

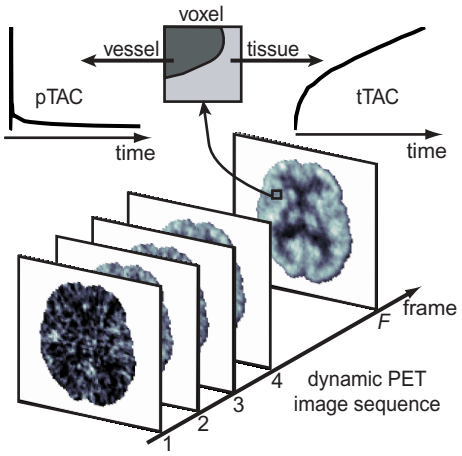

Fig. 1. Illustration of human brain FDG-PET image sequence. A voxel of FDG-PET image is a linear combination of pTAC and tTAC.

Table 1. Maximum and minimum inner products. All TACs (pTAC, tTACs) have unity norm.

	inner product	
	maximum	minimum
(1) pTAC and a group of tTACs	0.37	0.29
(2) one tTAC and the other tTACs	0.99	0.98

where K_1, k_2, and k_3 are parameters that describe the transfer rate of FDG. These parameters vary from voxel to voxel; therefore tTAC is not strictly common to all voxels. In order to examine the number of tTACs that should be assumed as the bases for independent maps, two similarities were examined: (1) between pTAC and a group of tTACs, and (2) between one tTAC and the other tTACs. tTACs were calculated using a measured pTAC and physiologically reasonable parameters, $K_1 = 1$, $k_2 = (0.08, 0.10, 0.12, 0.14)$, and $k_3 = (0.06, 0.08, 0.10, 0.12)$. Sixteen tTACs were calculated. Inner products using these tTACs and pTAC were calculated. The result is shown in Tab. 1. Whereas tTACs are similar to each other, and pTAC and a group of tTACs are dissimilar. Therefore the model that assumes two components (pTAC and tTAC components) is reasonable. A time–activity curve (TAC) is represented as a column vector, and each voxel's TAC, $\mathbf{x}(q)$, can be represented as:

$$\mathbf{x}(q) = s_{\rm p}(q)\mathbf{c}_{\rm p} + s_{\rm t}(q)\mathbf{c}_{\rm t} + \mathbf{n}(q), \tag{2}$$

where $s_{\mathrm{p}}(q)$ and $s_{\mathrm{t}}(q)$ are the qth voxel's value of the pTAC and tTAC maps, $\mathbf{c}_{\mathrm{p}}$ and $\mathbf{c}_{\mathrm{t}}$ are the pTAC and tTAC, respectively, and $\mathbf{n}(q)$ is a noise component. In matrix notation:

$$\mathbf{X} = \mathbf{c}_{\mathrm{p}}\mathbf{s}_{\mathrm{p}}^{\mathrm{T}} + \mathbf{c}_{\mathrm{t}}\mathbf{s}_{\mathrm{t}}^{\mathrm{T}} + [\mathbf{n}(1), \ldots, \mathbf{n}(q)] = \mathbf{CS} + \mathbf{N}, \quad (3)$$

where $\mathbf{s}_{\mathrm{p}}$ and $\mathbf{s}_{\mathrm{t}}$ are called the pTAC and tTAC maps, respectively. The pTAC map, $\mathbf{s}_{\mathrm{p}}$, corresponds to the blood volume image acquired with ^{15}O-CO inhalation, and the tTAC map, $\mathbf{s}_{\mathrm{t}}$, is determined by the scale of the tTAC and the ratio of tissue to the voxel.

3. METHODS

3.1. EPICA

The EPICA procedure consists of four steps:

Step 1. Append the negative images, $-\mathbf{X}$, to the measured PET images.

Step 2. Standardize each voxel's TAC using the time integral.

Step 3. Perform the fast fixed-point algorithm using the proposed cost function.

Step 4. Adjust the scale of the estimated pTAC using one-point blood sampling by arterial puncture.

Steps 1 and 2 are used as preprocessing for applying FastICA to the measured PET data. Step 3 extracts pTAC from dynamic PET images using FastICA. As ICA has an ambiguity in the scale of the estimated component, Step 4 determines the scale of the pTAC.

Step 1 forces the distributions of the pTAC and tTAC maps to be symmetric with zero mean.

$$\mathbf{X}_{\mathrm{N}} = [\mathbf{X}, -\mathbf{X}] = \mathbf{c}_{\mathrm{p}}[\mathbf{s}_{\mathrm{p}}^{\mathrm{T}}, -\mathbf{s}_{\mathrm{p}}^{\mathrm{T}}] + \mathbf{c}_{\mathrm{t}}[\mathbf{s}_{\mathrm{t}}^{\mathrm{T}}, -\mathbf{s}_{\mathrm{t}}^{\mathrm{T}}] \quad (4)$$

In Step 2, the difference between the probability distributions of pTAC and tTAC maps is enhanced by standardization as shown in Fig. 2. The enhanced TAC, $x_{\mathrm{E}}(q, f)$, is given as below:

$$x_{\mathrm{E}}(q, f) = \frac{x(q, f)}{\left| \int_0^F x(q, f) \mathrm{d}f \right|}. \quad (5)$$

As pharmaceutical administration is performed by a bolus injection to the antecubital vein, pTAC has a pulse-like shape. And the ratio of the vessel's volume to each voxel is very small. Therefore, the time integral of tTAC is much larger than that of pTAC in almost all voxels. Standardization using the time integral is nearly equal to standardization using the tTAC

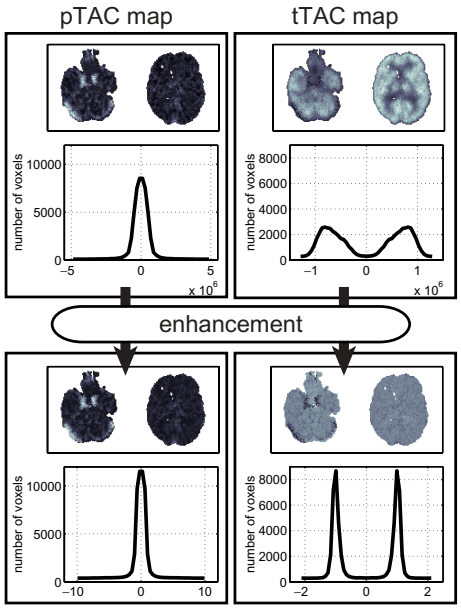

Fig. 2. Histograms of the original pTAC and tTAC maps and the enhanced pTAC and tTAC maps.

time integral. Therefore, the pTAC map is converted to the heavy tailed distribution and the tTAC map is concentrated to around 1 or -1 during Step 2 (Fig. 2). Step 2 is intended to convert an unknown distribution in the measured dynamic PET images to a statistically characterized distribution that is utilized to design a contrast function at Step 3. Step 3 applies the fast fixed-point algorithm to the PET images preprocessed by Steps 1 and 2. Each TAC is normalized under the L1 norm by Step 2 and each map is normalized under the L2 norm by whitening. The contrast function is sensitive to the heavy tailed distribution and has the penalty term that prevents the voxel values from being concentrated close to zero.

$$G(u) = u^6 - \frac{\lambda}{k} \exp\left(-\frac{|u|}{k}\right), \quad (6)$$

where u is the whitened PET images, and λ and k are positive parameters. The pTAC-related component is estimated by maximizing the contrast function (6).

3.2. ICA with Nonnegative Constraint by EL

EL [12] is a recently developed method for approximating an intractable actual posterior distribution by factorial simpler distributions. The priors for the mixing matrix and the source images are assumed to be a rectified Gaussian and an exponential distribution, re-

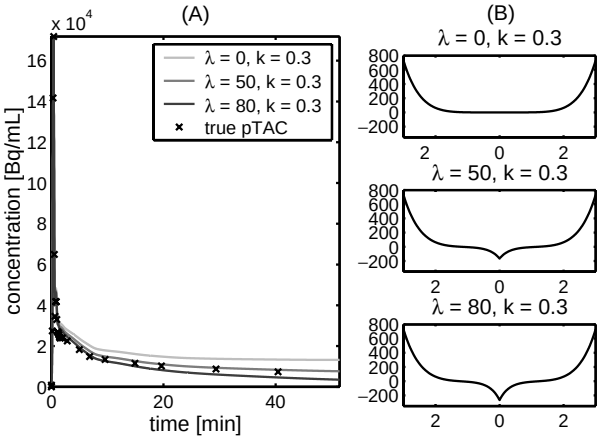

Fig. 3. (A) The estimated pTACs using EPICA from the simulated FDG-PET images and (B) the corresponding cost functions. The parameters of the cost functions are $(\lambda, k) = (0, 0.3), (50, 0.3), (80, 0.3)$. True pTAC is shown with crosses.

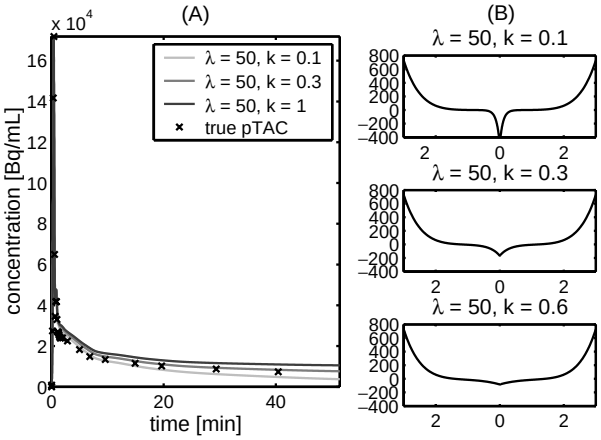

Fig. 4. (A) The estimated pTACs using EPICA from the simulated FDG-PET images and (B) the corresponding cost functions. The parameters of the cost functions are $(\lambda, k) = (50, 0.1), (50, 0.3), (50, 0.6)$. True pTAC is shown with crosses.

spectively, to incorporate the nonnegative constraint.

$$p\left(c_i(f)\right) = G^{(R)}\left(c_i(f)|0, \beta_i\right) \quad (7)$$

$$G^{(R)}\left(c_i(f)|a, b\right) \propto \begin{cases} \exp\left(-\frac{b}{2}\left(c_i(f)-a\right)^2\right) & \text{if } c_i(f) \geq 0 \\ 0 & \text{if } c_i(f) < 0 \end{cases} \quad (8)$$

$$p\left(s_i(q)\right) = \begin{cases} \frac{1}{d}\exp\left(-\frac{s_i(q)}{d}\right) & \text{if } s_i(q) \geq 0 \\ 0 & \text{if } s_i(q) < 0 \end{cases} \quad (9)$$

The noise, $n(q, f)$, is assumed to be additive Gaussian noise.

$$p(\mathbf{x}(q)|\mathbf{s}(q), \mathbf{C}, \Sigma) = G(\mathbf{x}(q)|\mathbf{C}\mathbf{s}(q), \Sigma) \quad (10)$$

Using these priors, EL minimizes the mismatch between the posterior distribution, $P(\mathbf{s}, \mathbf{C}, \beta, d, \Sigma|\mathbf{x}, H)$ (H denotes the model) and the approximating distribution, $Q(\mathbf{s}, \mathbf{C}, \beta, d, \Sigma)$.

4. EXPERIMENTAL RESULTS

4.1. Simulation: Parameters of the Cost Function

The influence of the parameters in (6) on an extracted pTAC was investigated using computer-generated images. The simulated data were generated based on measured PET data. FDG-PET scans were performed on volunteers using a Headtome-V scanner (Shimadzu Corp., Japan) in 2D mode. The simulated PET images have 24 frames and seven slices, each of which has 128 $\times$ 128 voxels. Serial arterial plasma sampling was performed simultaneously. Kinetic parameters, (K_1, k_2, k_3), of each voxel's TAC in (1) were estimated and the noise-free tTACs were calculated using the estimated kinetic parameters and the measured pTAC based on (1). The noise-free simulated data were generated using the equation:

$$x_{\text{sim}}(q, f) = V_{\text{B}}(q)c_{\text{p}}(f) + (1 - V_{\text{B}}(q))c_{\text{t}}(q, f), \quad (11)$$

where $V_{\text{B}}(q)$ is the blood volume, $c_{\text{p}}(f)$ is the measured pTAC, and $c_{\text{t}}(q, f)$ is the calculated noise-free tTAC. The Gaussian noise, $n(q, f)$, was added to the noise-free simulated data. It was assumed to be represented by the equation:

$$n(q, t) \sim N\left(0, \alpha\frac{x_{\text{sim}}(q, f)}{\delta f}\right), \quad (12)$$

where α is the noise level and δf is the width of a frame. The noise level was set to 30.

EPICA was applied to the simulated PET images in two cases: (Case 1) λ was varied from 0 to 100 in steps of 10 and k was fixed at 0.3, and (Case 2) λ was fixed at 50 and k was varied from 0.1 to 1 in steps of 0.1. Figures 3 and 4 show the estimated pTACs using EPICA from the simulated PET data and the cost functions. As the value of λ increases and the value of k decreases, i.e., the contribution of the penalty term to the contrast function increases, the tail of the estimated pTAC decreases more rapidly.

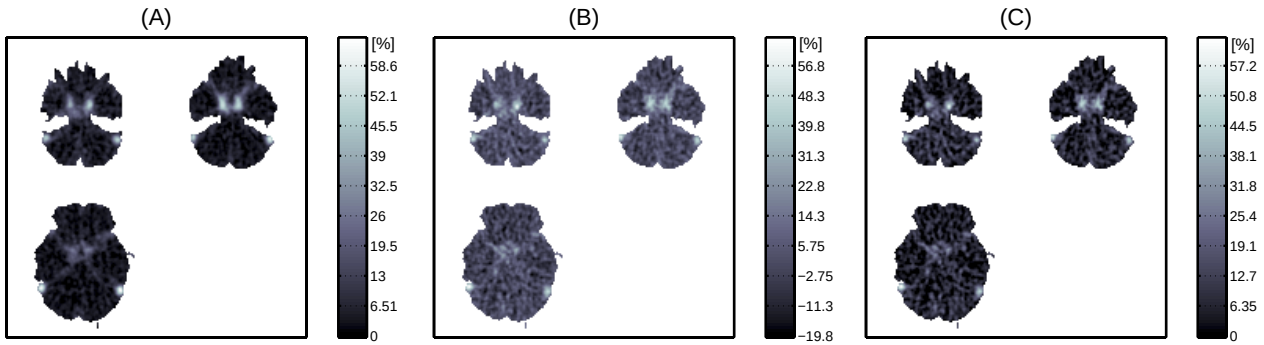

Fig. 5. (A) Blood volume image measured with ^{15}O-CO inhalation. (B) pTAC map estimated using EPICA. (C) pTAC map estimated using EL.

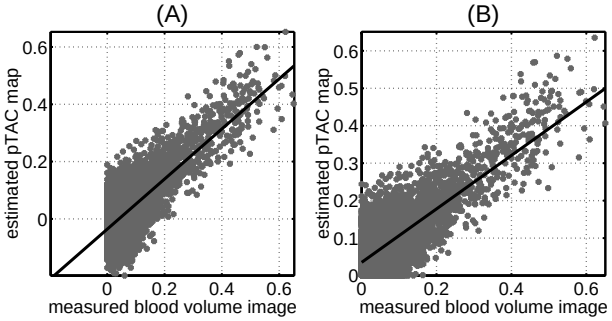

Fig. 6. Scatter plots between the blood volume image and the estimated pTAC map using (A) EPICA and (B) EL.

4.2. Human FDG-PET Experiment

EPICA and EL were applied to the measured PET data. The number of frames was 27, and the frame arrangements were 10 s × 6, 30 s × 3, 1 min × 5, 2.5 min × 5, and 5 min × 8. Thirty slices, each of which has 128 × 128 voxels, were scanned. The 24 arterial blood samples were taken simultaneously via an inserted catheter in the brachial artery. The blood volume images were also scanned with ^{15}O-CO inhalation. By performing PCA, the dimension of PET images was reduced to two before applying EPICA or EL. In EPICA, all voxels were used for the estimation and three slices were used for EL. The parameters of the contrast function in (6) were $\lambda = 100$, $k = 0.3$.

Figure 5 shows the measured blood volume image and the estimated pTAC maps; figure 6 shows the scatter plots between the measured blood volume image and the estimated pTAC maps by EPICA (A) and EL (B). Correlation coefficients between the measured blood volume image and the pTAC maps estimated by

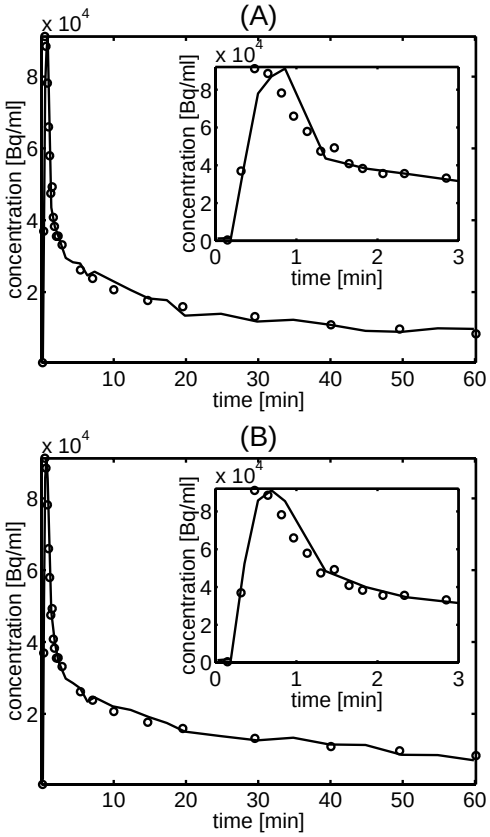

Fig. 7. Estimated pTACs by (A) EPICA (solid line) and (B) EL (solid line). The measured pTAC was plotted with open circles. A magnified view of the first 3 min of the estimated pTAC is shown in the inset.

EPICA and EL were 0.71 ($y = 0.87x - 0.036$) and 0.87 ($y = 0.71x + 0.035$), respectively. Figure 7 shows the estimated pTACs by EPICA (A) and EL (B). The scale

of the estimated pTACs was adjusted by the peak value of the measured pTAC. The calculation time was 10 sec in EPICA and 4000 sec in EL.

5. DISCUSSION

We have investigated the way in which parameters of the contrast function in EPICA affect the estimated pTAC using simulated FDG-PET data. Figures 3 and 4 show that the penalty term of the contrast function determines the tail of the estimated pTAC. In this paper, the possibility of a nonnegative constraint was also examined. As shown in Fig. 7, the estimated pTACs by EPICA and EL were similar to the measured pTAC. The blood volume image estimated by EL had nonnegative voxels whereas that estimated by EPICA included negative voxels. There was a direct correspondence between the voxel values of the two pTAC maps (Fig. 6). EL, with nonnegative priors, calculated the nonnegative blood volume image while maintaining the accuracy of the pTAC estimation, compared with that using EPICA. EL, however, requires greater computational time; the reduction of calculation time will be therefore the subject of future work.

6. REFERENCES

[1] S. C. Huang, M. E. Phelps, E. J. Hoffman, K. Sideris, C. J. Selin, and D. E. Kuhl, "Noninvasive determination of local cerebral metabolic rate of glucose in man," *Am. J. Physiol.*, vol. 238, no. 1, pp. E69–E82, January 1980.

[2] P. H. Jons, M. Ernst, J. Hankerson, K. Hardy, and A. J. Zametkin, "Follow-up of radial arterial catheterization for positron emission tomography studies," *Hum. Brain Mapp.*, vol. 5, no. 2, pp. 119–123, 1997.

[3] R. F. Bedford and H. Wollman, "Complications of percutaneous radial-artery cannulation: an objective prospective study in man," *Anesthesiology*, vol. 38, no. 3, pp. 228–236, March 1973.

[4] D. C. Barber, "The use of principal components in the quantitative analysis of gamma camera dynamic studies," *Phys. Med. Biol.*, vol. 25, no. 2, pp. 283–292, 1980.

[5] R. Di Paola, J. P. Bazin, F. Aubry, A. Aurengo, F. Cavailloles, J. Y. Herry, and E. Kahn, "Handling of dynamic sequences in nuclear medicine," *IEEE Trans. Nucl. Sci.*, vol. NS–29, no. 4, pp. 1310–1321, August 1982.

[6] H.-M. Wu, C. K. Hoh, Y. Choi, H. R. Schelbert, R. A. Hawkins, M. E. Phelps, and S.-C. Huang, "Factor analysis for extraction of blood time-activity curves in dynamic FDG–PET studies," *J. Nucl. Med.*, vol. 36, no. 9, pp. 1714–1722, September 1995.

[7] W. R. Martin, W. J. Powers, and M. E. Raichle, "Cerebral blood volume measured with inhaled $C^{15}O$ and Positron Emission Tomography," *J. Cereb. Blood Flow Metab.*, vol. 7, no. 4, pp. 421–426, 1987.

[8] M. J. McKeown, S. Makeig, G. G. Brown, T.-P. Jung, S. S. Kindermann, A. J. Bell, and T. J. Sejnowski, "Analysis of fMRI data by blind separation into independent spatial components," *Hum. Brain Mapp.*, vol. 6, pp. 160–188, 1998.

[9] M. Naganawa, A. Matani, and Y. Kimura, "Extraction of vessel-related information from PET images without continuous blood sampling using modified independent component analysis," in *Proc. IEEE EMBC*, Istanbul, 2001, CD-ROM.

[10] A. Hyvärinen and E. Oja, "A fast fixed-point algorithm for independent component analysis," *Neural Comput.*, vol. 9, no. 7, pp. 1483–1492, 1997.

[11] M. Naganawa, Y. Kimura, K. Ishii, K. Oda, K. Ishiwata, and A. Matani, "Extraction of a plasma time-activity curve from dynamic brain PET images based on independent component analysis," *IEEE Trans. Med. Imag.*, 2002, submitted.

[12] J. Miskin and D. J. C. MacKay, *Advances in independent component analysis*, chapter Ensemble learning for blind image separation and deconvolution, pp. 123–141, Springer, 2000.